Supporting information

Polyoxometalate-Based Metal-Organic Coordination Networks for Heterogeneous Catalytic Desulfurization

Yuan-Yuan Ma,[a] Hua- Qiao Tan,*[a] Yong-Hui Wang,[a] Xiu-Li Hao,*[a,b] Xiao-Jia Feng, [a,c] Hong-Ying Zang,[a] and Yang-Guang Li*[a]

[a]*Key Laboratory of Polyoxometalate Science of Ministry of Education, Faculty of Chemistry, Northeast Normal University, Renmin Street No. 5268, Changchun, Jilin 130024, P.R. China*

[b]*School of Chemical and Biological Engineering, Taiyuan University of Science and Technology, Taiyuan 030021, PR China*

[c] *College of Science, Shenyang Agricultural University, Shenyang, 110866, P.R. China*

Contents

1.Additional structural figures for compound 1-3

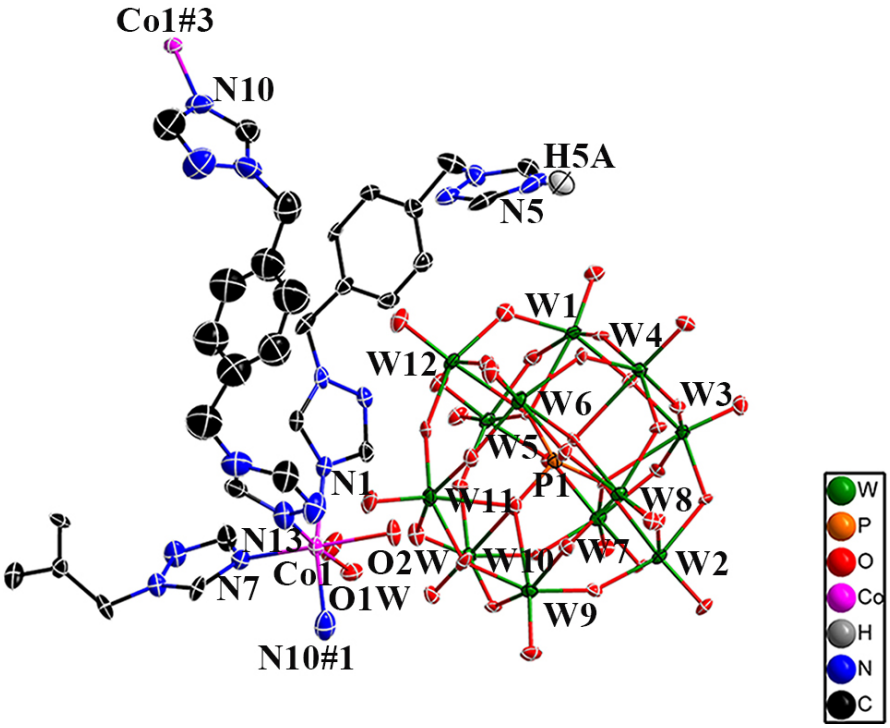

Figure. S1 ORTEP diagram of the basic structural units in **compound 1** with thermal ellipsoids at 30% probability displacement. (symmetry codes: #1 x,-y+1,z+1/2; #2 -x,y,-z-1/2; #3 x,-y+1,z-1/2).

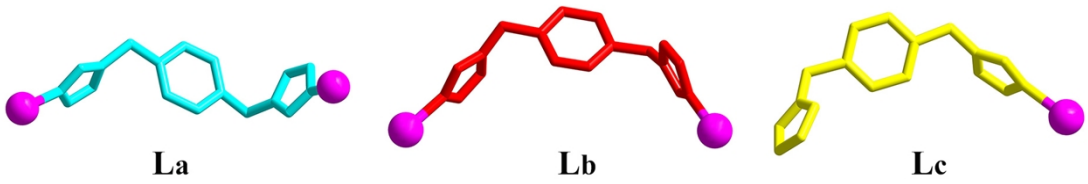

Figure. S2 The three groups of BBTZ ligands labeled with L_a, L_b and L_c in this metal-organic cationic moiety of **compound 1**.

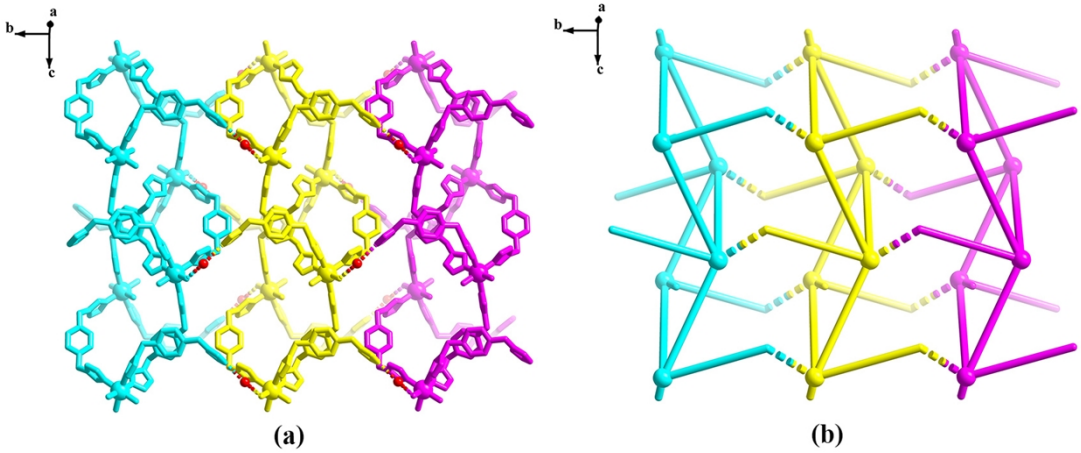

Figure. S3 a) The 2-D network in **compound 1** viewed along *a* axis. 1-D ladder-like chains are shown with yellow, blue and purple color for clarity. The lattice water molecules are shown with red ball. **b)** Schematic view of the 2-D network topology in **compound 1** viewed along *a* axis.

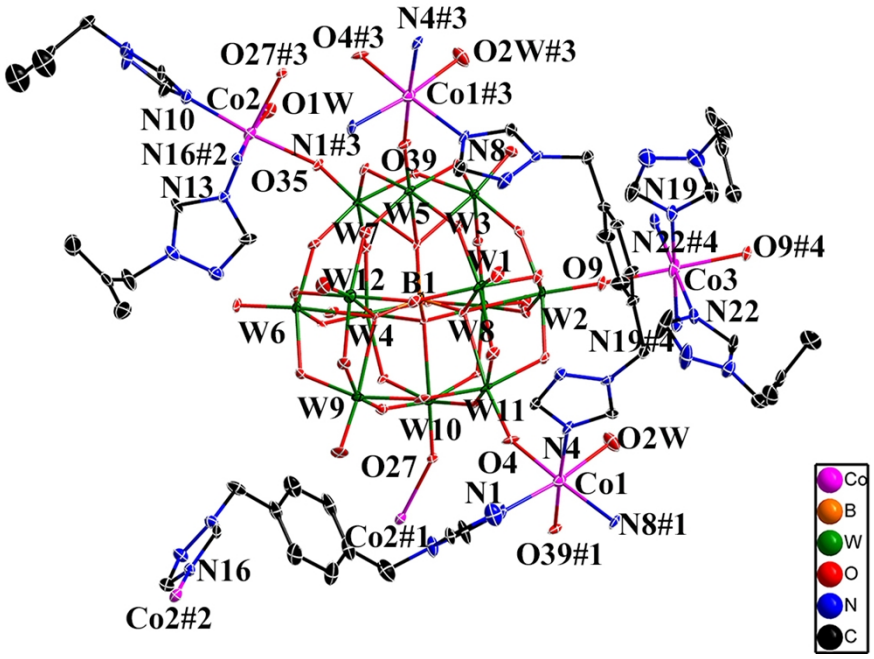

Figure. S4 ORTEP diagram of the basic structural units in **compound 2** with thermal ellipsoids at 30% probability displacement. All H atoms are omitted for clarity. (symmetry codes: #1 x+1,y,z; #2 -x+2,-y+1,-z+1; #3 x-1,y,z; #4 -x+2,-y+1,-z+2).

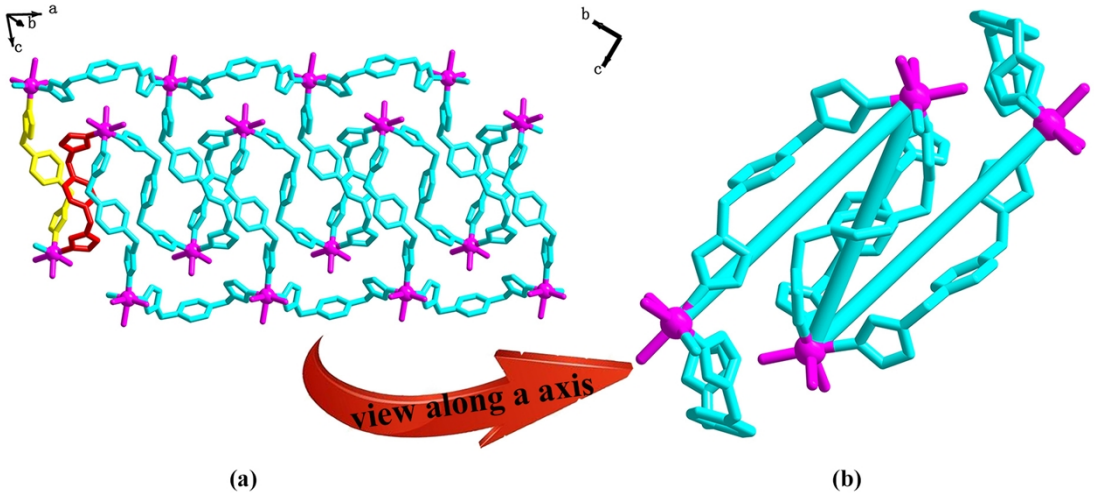

Figure. S5 The 1D metal-organic chains with the "N"-type cross-section viewed along *a* axis in **compound 2**.

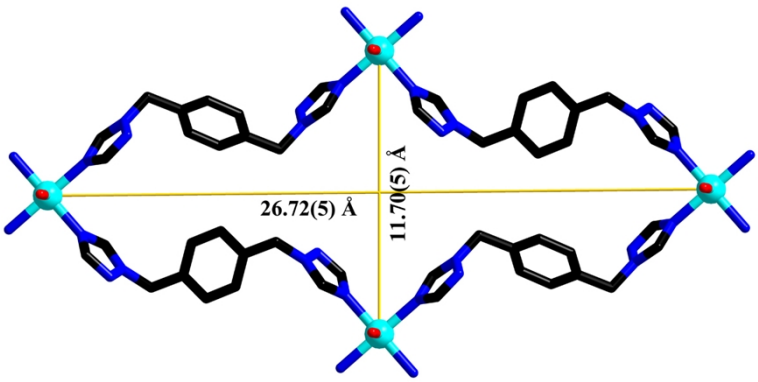

Figure. S6 mesh of 2D (4^4) *sqp* network with the size of 11.70(5) × 26.72(5) Å in **compound 2**.

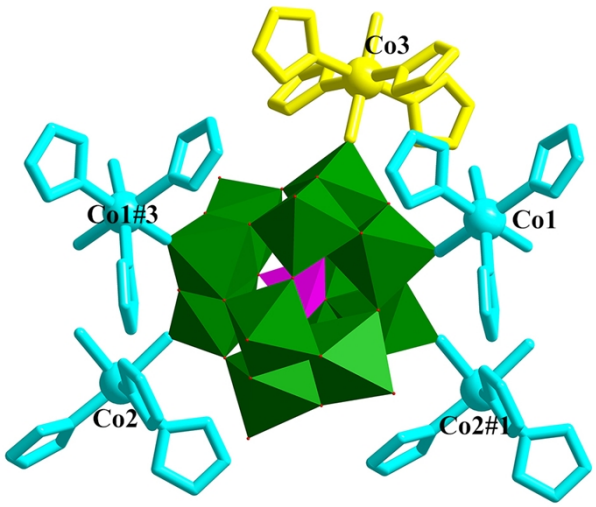

Figure. S7 The coordination environment of BW_{12} (the five connected node) anion in **compound 2.** (symmetry codes: #1 x+1,y,z; #3 x-1,y,z).

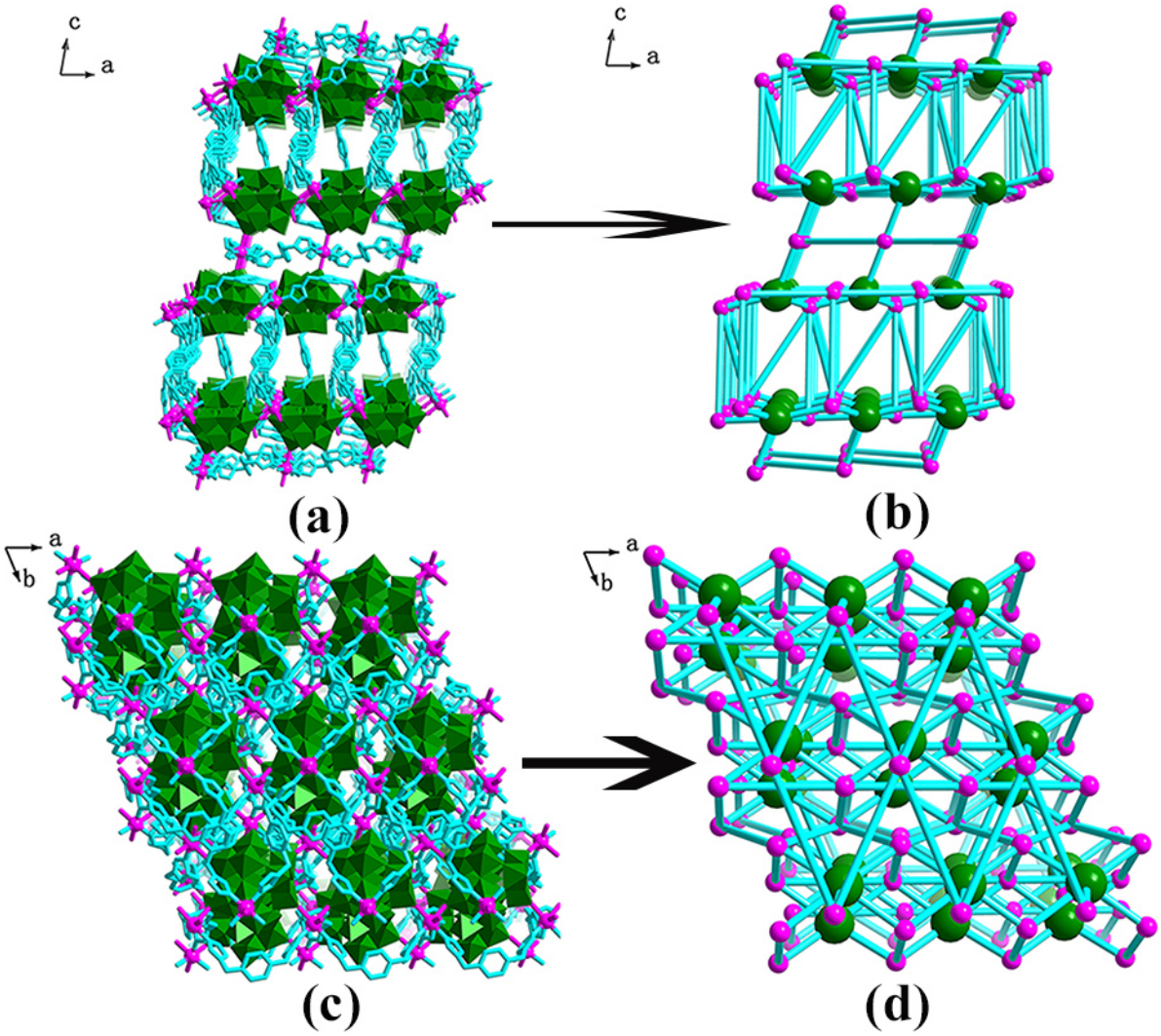

Figure. S8 **a)** The chemical and **b)** schematic views of the POM-supported 3D network of **compound 2** viewed along b axis; **c)**the chemical and **d)** schematic view of the POM-supported 3D network along c axis.

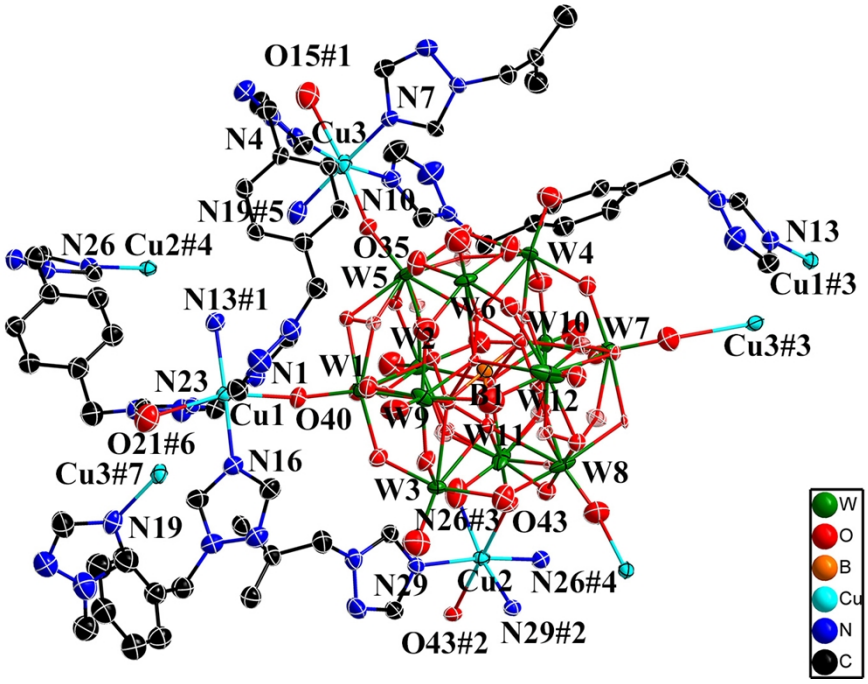

Figure. S9 ORTEP diagram of the basic structural units in **compound 3** with thermal ellipsoids at 30% probability displacement. All H atoms are omitted for clarity. (symmetry codes: #1 x,-y+1,z+1/2; #2 -x+1,y,-z+1/2; #3 x,-y+1,z-1/2; #4 -x+1,-y+1,-z+1; #5 x,y+1,z; #6 x,-y,0.5+z; #7 x,y-1,z).

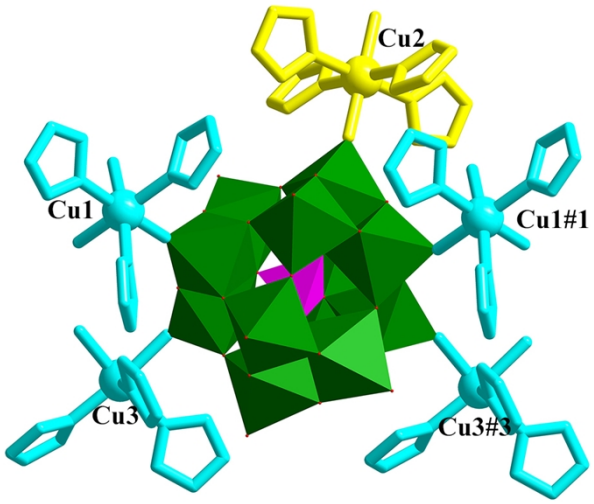

Figure. S10 The coordination environment of BW_{12} (the five connected node) anion in **compound 3.** (symmetry codes: #1 x,-y+1,z+1/2; #2 -x+1,y,-z+1/2; #3 x,-y+1,z-1/2).

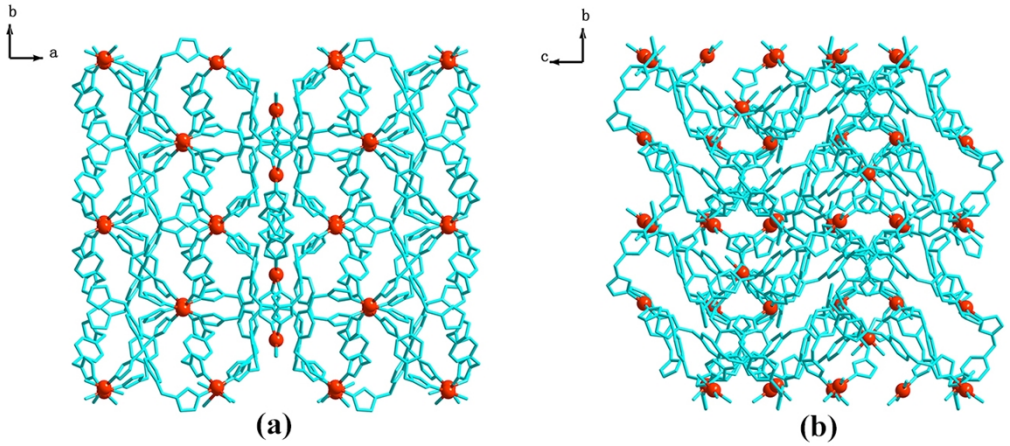

Figure. S11 The chemical views of the 3-D metal-organic network in **compound 3** viewed along **a)** c axis and **b)** a axis.

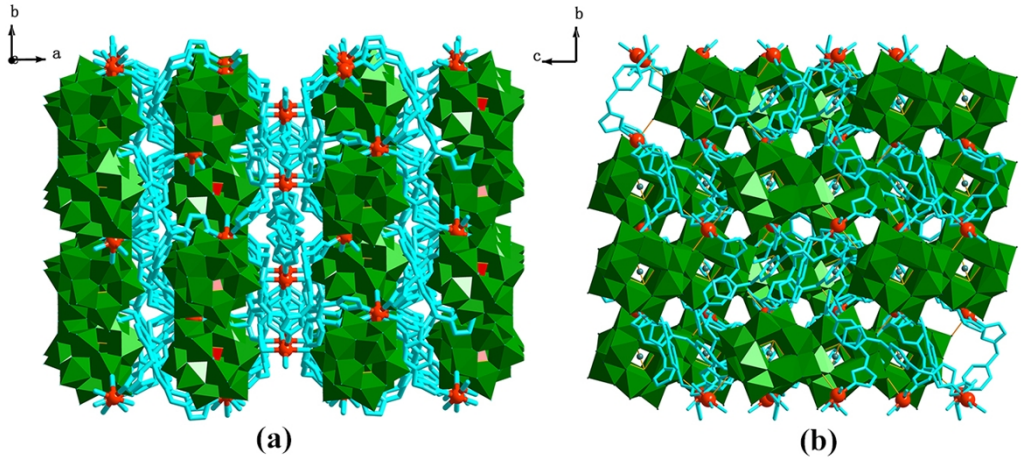

Figure. S12 The chemical views of the POM-supported 3D open framework in **compound 3** viewed along **a)** c axis and **b)** a axis.

2. Selected bond lengths and angles for compounds 1-3

Table S1. Selected bond lengths (Å) and angles (deg) of **compound 1.**

Co(1)-N(1)	2.191(9)	Co(1)-N(7)	2.086(9)
Co(1)-N(10)#1	2.18(11)	Co(1)-N(13)	2.097(12)
Co(1)-O(1W)	2.139(13)	Co(1)-O(2W)	2.089(12)
N(1)-Co(1)-N(7)	93.2(4)	N(1)-Co(1)-N(10)#1	169(3)
N(1)-Co(1)-N(13)	92.1(6)	N(1)-Co(1)-O(1W)	83.0(5)
N(1)-Co(1)-O(2W)	83.9(5)		

Symmetry transformations used to generate equivalent atoms: #1 x,-y+1,z+1/2.

Table S2. Selected bond lengths (Å) and angles (deg) of **compound 2**.

Co(1)-N(1)	2.094(6)	Co(1)-N(4)	2.105(6)
Co(1)-N(8)#1	2.126(6)	Co(1)-O(4)	2.125(8)
Co(1)- O(39)#1	2.084(7)	Co(1)-O(2W)	2.174(9)
Co(2)-N(10)	2.096(6)	Co(2)-N(16)#2	2.136(6)
Co(2)-N(13)	2.113(6)	Co(2) - O(35)	2.117(8)
Co(2)-O(27)#3	2.167(8)	Co(2)-O(1W)	2.067(8)
Co(3)-N(19)	2.108(6)	Co(3)-N(19)#4	2.108(6)
Co(3)-N(22)	2.116(6)	Co(3)-N(22)#4	2.116(6)
Co(3)-O(9)	2.147(8)	Co(3)-O(9)#4	2.147(8)
N(1)-Co(1)-N(4)	93.4(3)	N(1)-Co(1)-N(8)#1	98.1(3)
N(1)-Co(1)-O(4)	89.3(3)	N(1)-Co(1)-O(2W)	171.7(4)
N(1)-Co(1)-O(39)#1	91.6(3)	N(10)-Co(2)-N(13)	94.4(3)
N(10)-Co(2)-O(1W)	87.8(3)	N(10)-Co(2)-O(35)	174.4(3)
N(10)-Co(2)-N(16)#2	96.6(3)	N(10)-Co(2)-O(27)#3	90.8(3)
N(19)-Co(3)-N(19)#4	180	N(19)-Co(3)-N(22)#4	90.9(3)
N(19)-Co(3)-N(22)	89.1(3)	N(19)-Co(3)-O(9)#4	92.6(3)
N(19)-Co(3)-O(9)	87.4(3)		

Symmetry transformations used to generate equivalent atoms: #1 x+1,y,z; #2 -x+2,-y+1,-z+1; #3 x-1,y,z; #4 -x+2,-y+1,-z+2.

Table S3. Selected bond lengths (Å) and angles (deg) of **compound 3**.

Cu(1)-N(1)	2.004(13)	Cu(1)-N(16)	2.013(13)
Cu(1)-N(23)	2.017(11)	Cu(1)-N(13)#1	2.022(12)
Cu(1)-O(40)	2.294(18)	Cu(2)-O(43)	2.211(16)
Cu(2)-N(29)	2.050(17)	Cu(2)-N(29)#2	2.050(17)
Cu(2)-N(26)#3	2.06(3)	Cu(2)-N(26)#4	2.06(3)
Cu(2)-O(43)#2	2.211(16)	Cu(3)-O(35)	2.421(17)
Cu(3)-N(7)	1.947(11)	Cu(3)-N(19)#5	1.949(16)
Cu(3)-N(4)	2.013(12)	Cu(3)-N(10)	2.016(12)
N(1)-Cu(1)-N(16)	92.0(7)	N(1)-Cu(1)-N(23)	175.3(7)
N(1)-Cu(1)-N(13)#1	88.9(7)	N(1)-Cu(1)-O(40)	93.8(7)
N(29)-Cu(2)-N(29)#2	90.3(11)	N(29)-Cu(2)-N(26)#3	92.0(14)
N(29)-Cu(2)-N(26)#4	167.7(14)	N(29)-Cu(2)- O(43)	93.8(6)
N(29)-Cu(2)-O(43)#2	84.7(6)	N(7)-Cu(3)-N(4)	86.7(7)
N(7)-Cu(3)-N(10)	88.5(7)	N(7)-Cu(3)-N(19)#5	177.8(8)
N(7)-Cu(3)-O(35)	92.1(6)		

Symmetry transformations used to generate equivalent atoms: #1 x,-y+1,z+1/2; #2 -x+1,y,-z+1/2; #3 x,-y+1,z-1/2; #4 -x+1,-y+1,-z+1; #5 x,y+1,z

3. Catalytic experiments for compound 1-3

3.1 The confirmation of the products

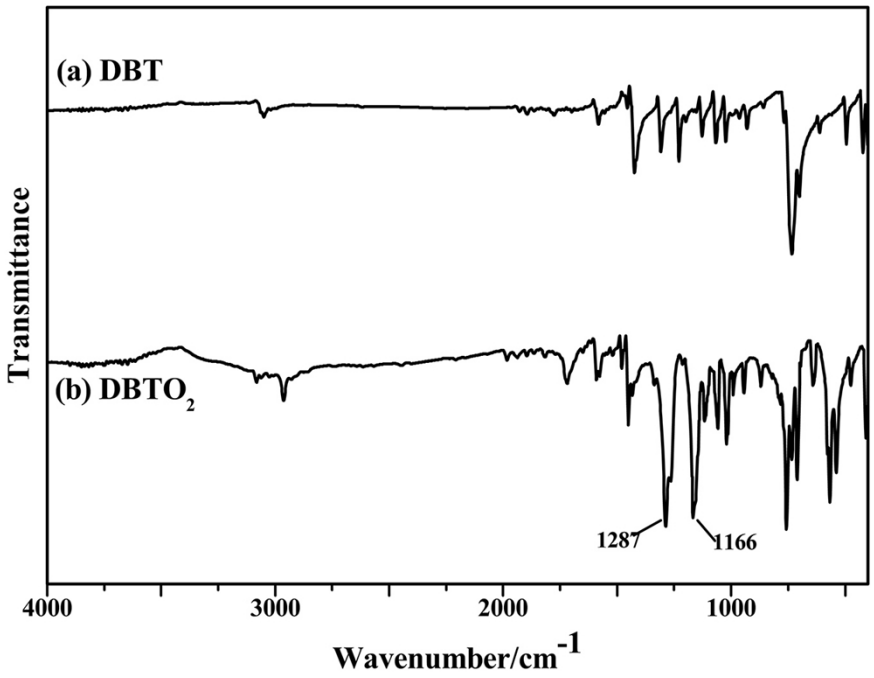

Figure. S13 FTIR spectrum of DBT and oxidation reaction product $DBTO_2$.The appearance of characteristic frequencies at 1287 cm^{-1} (ν_{as}, SO_2) and 1166 cm^{-1} (ν_s, SO_2) confirm the occurrence of sulfones as the product.

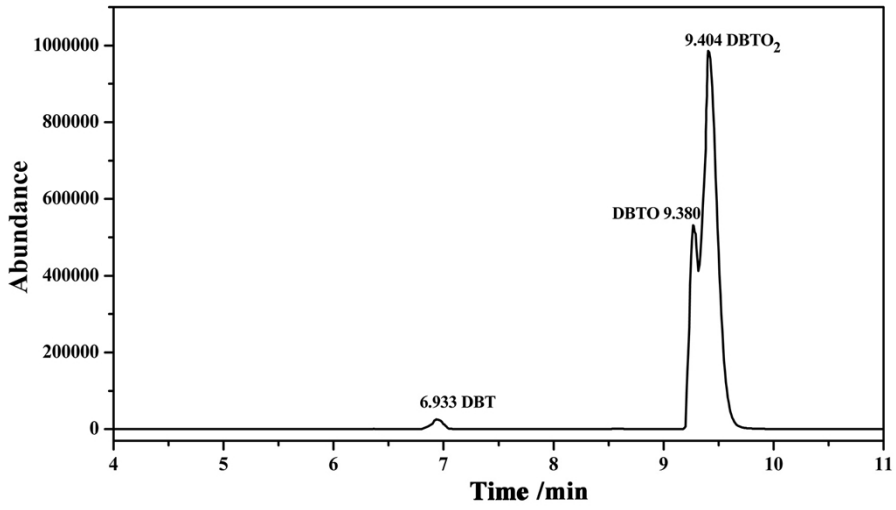

Figure. S14 GC trace of the catalytic results for the oxidation of DBT.

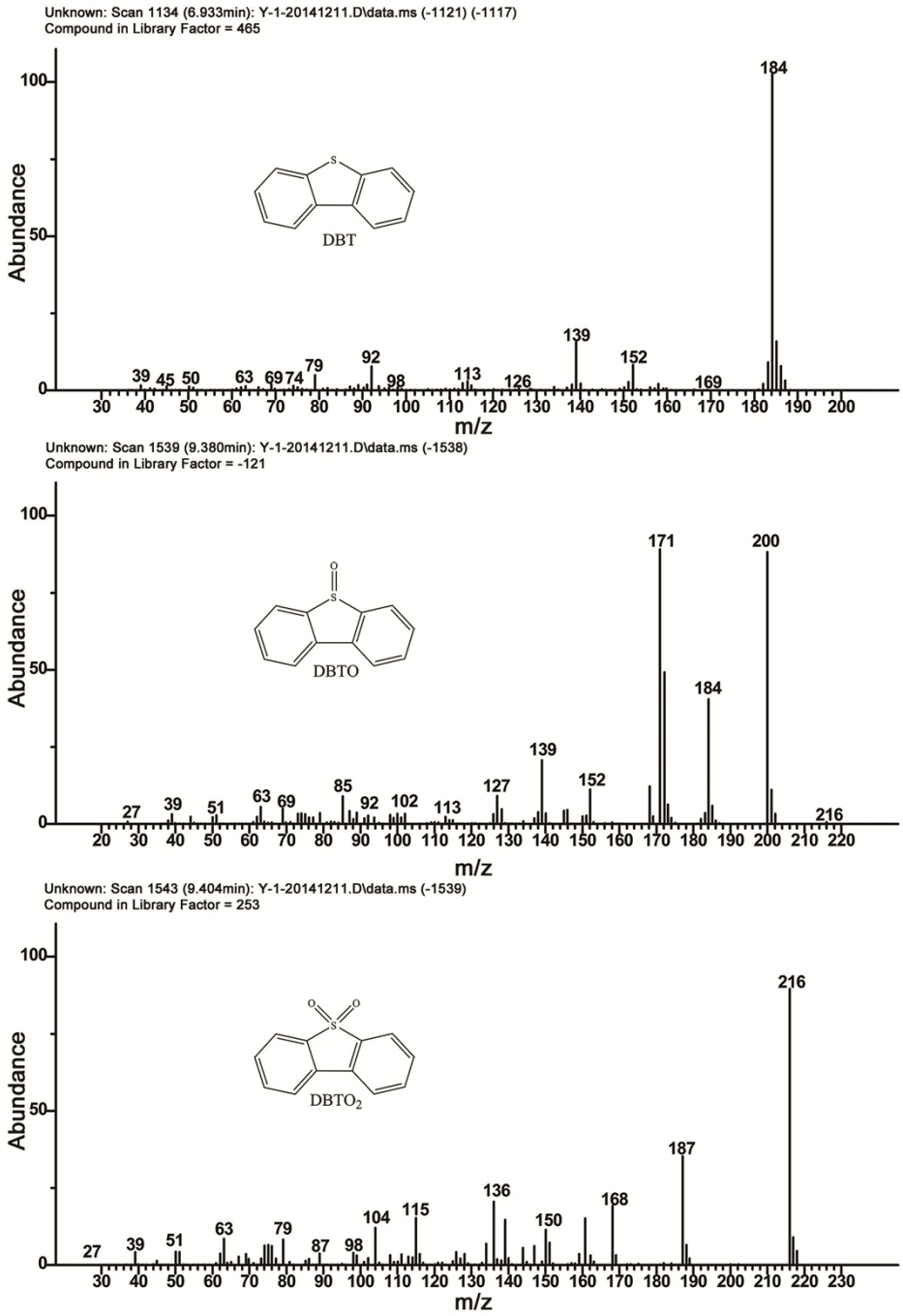

Figure. S15 MS spectra for the oxidation products of DBT and unreacted DBT.

3.2 The catalytic oxidation experiments of DBT

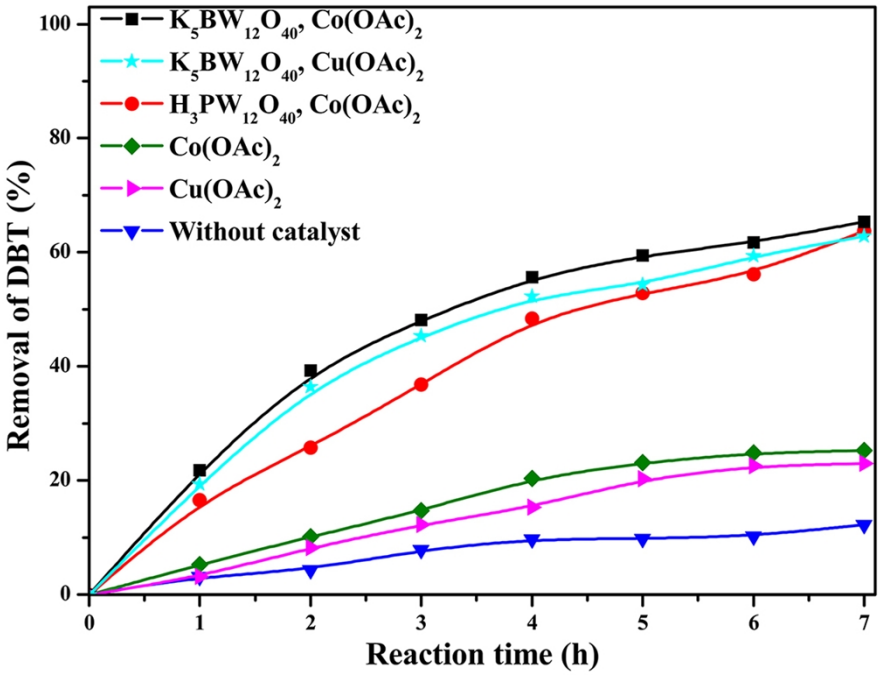

Figure. S16 Removal of DBT versus reaction time with the solid precursors as catalysts.

Table S4. The catalytic activities of POM-based MOCNs catalysts.

Catalysts	Loading amount of POM	oxidant	Reaction time / h	Conversion of DBT /%	Reference
$[(CH_3)_4N]_2\{[Cu_2(BTC)_{4/3}(H_2O)_2]_6[H_3PV_2Mo_{10}O_{40}]\}\cdot 14H_2O$	36.17%	O_2	1.5	41	ChemCatChem 2013, 5, 3086 – 3091
$[Co(BBPTZ)_3][HPMo_{12}O_{40}]\cdot 24H_2O$	71%	TBHP	8	99.16	Chem. Eur. J. 2015, 21, 3778 – 3784
$[Co(HBBTZ)(BBTZ)_{2.5}][PMo_{12}O_{40}]$	66.95%	TBHP	9	98.1	Chem. Eur. J. 2015, 21, 3778 – 3784
Compound 1	80.10 %	TBHP	7	91.57	This article
Compound 2	70.13 %	TBHP	7	99.63	This article
Nano-compound 2	70.13 %	TBHP	3	99.74	This article
Compound 3	67.17 %	TBHP	7	96.68	This article

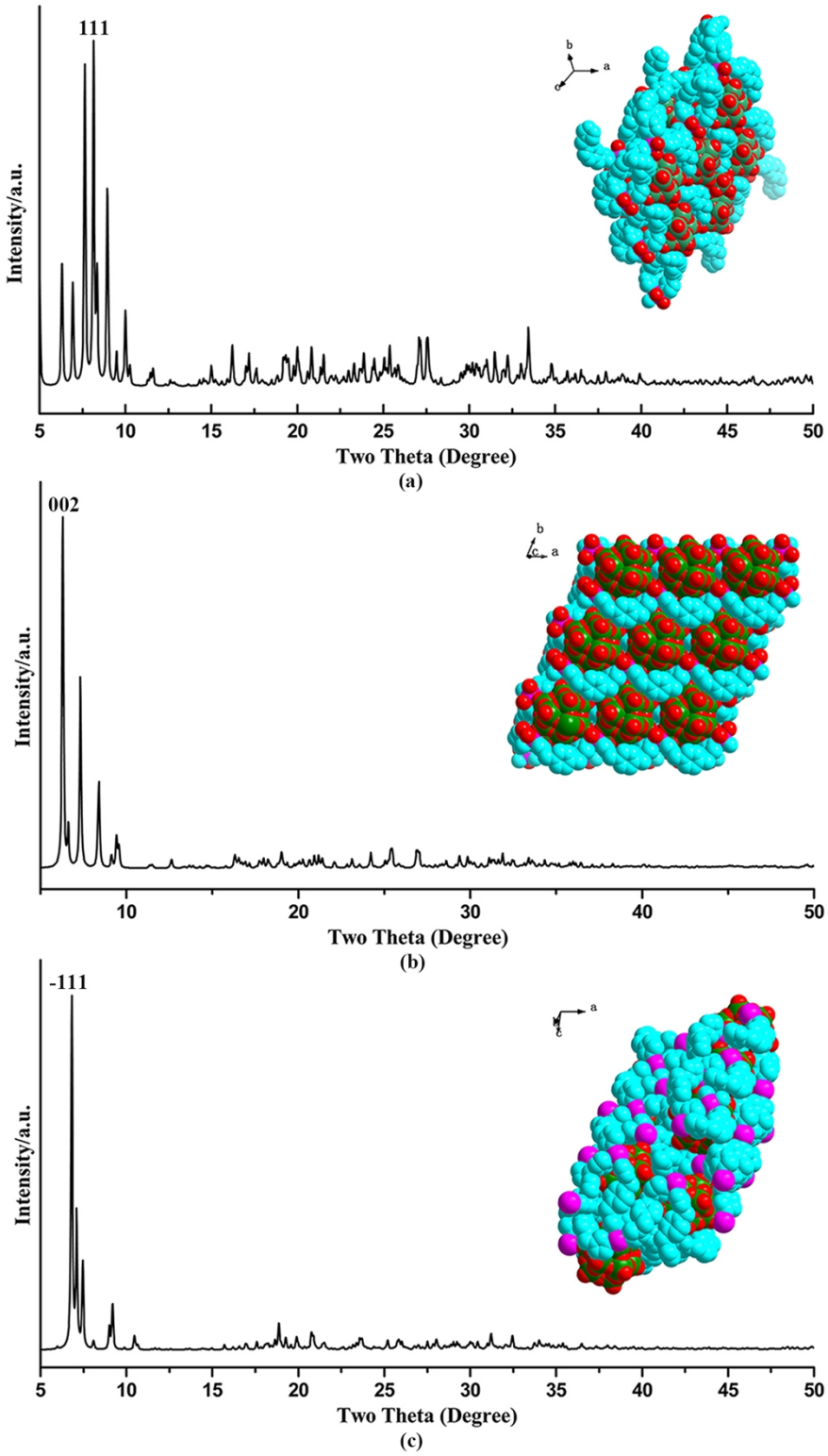

Figure. S17 a) the advantage {111} facets in the XRD of **1**, (inset: the space filling structure of advantage {111} facets in **1**; **b)** the advantage {002} facets in the XRD of **2**, (inset: the space filling structure of advantage {002} facets in **2**; **c)** advantage {-111} facets in the XRD of **3**, (inset: the space filling structure of advantage {-111} facets in **3**.

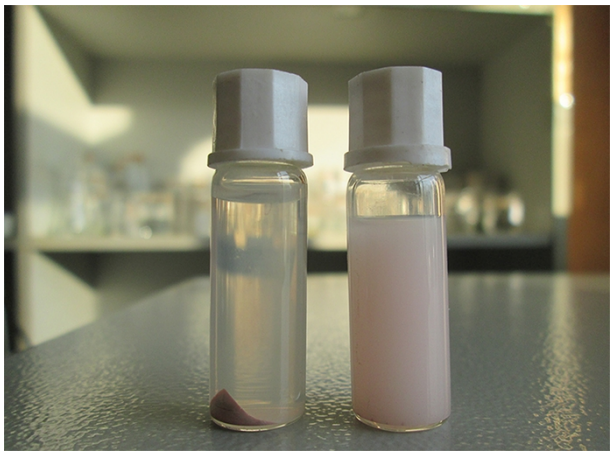

Figure. S18 (a) catalyst can be recovered from the reaction vessel by centrifugal separation; (b) nanocrystal **2** dispersed in reaction system.

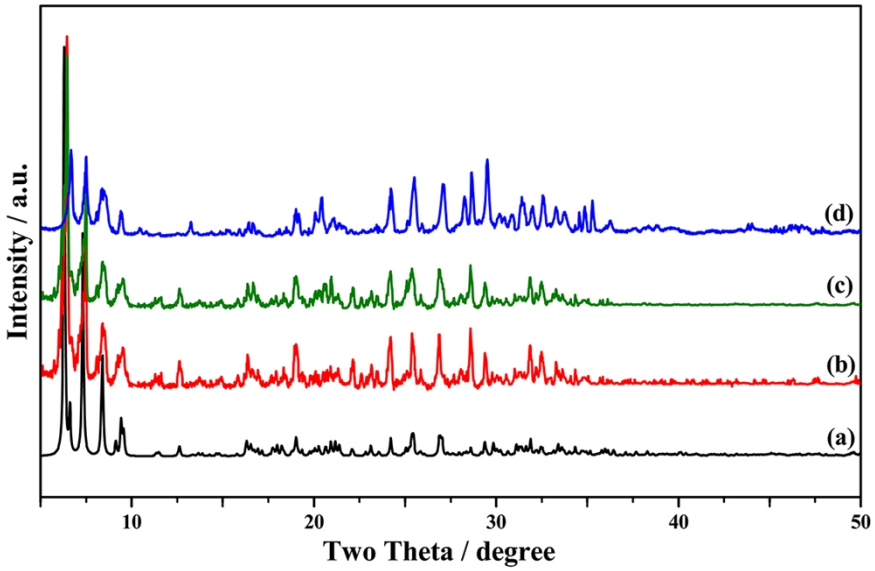

Figure. S19 XPRD patterns of **compound 2**: (a) simulated, (b) as-synthesized, (c) nanocrystal **2**, (d) nanocrystal **2** after catalytic reaction.

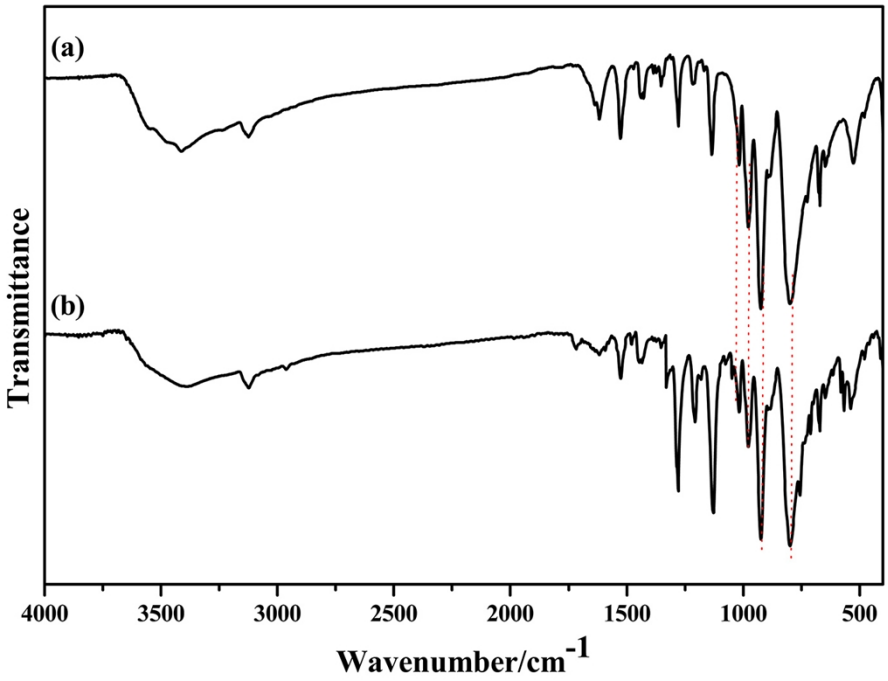

Figure. S20 FT/IR spectrum of nanocrystal **2** (a)before catalysis; (b) after catalysis.

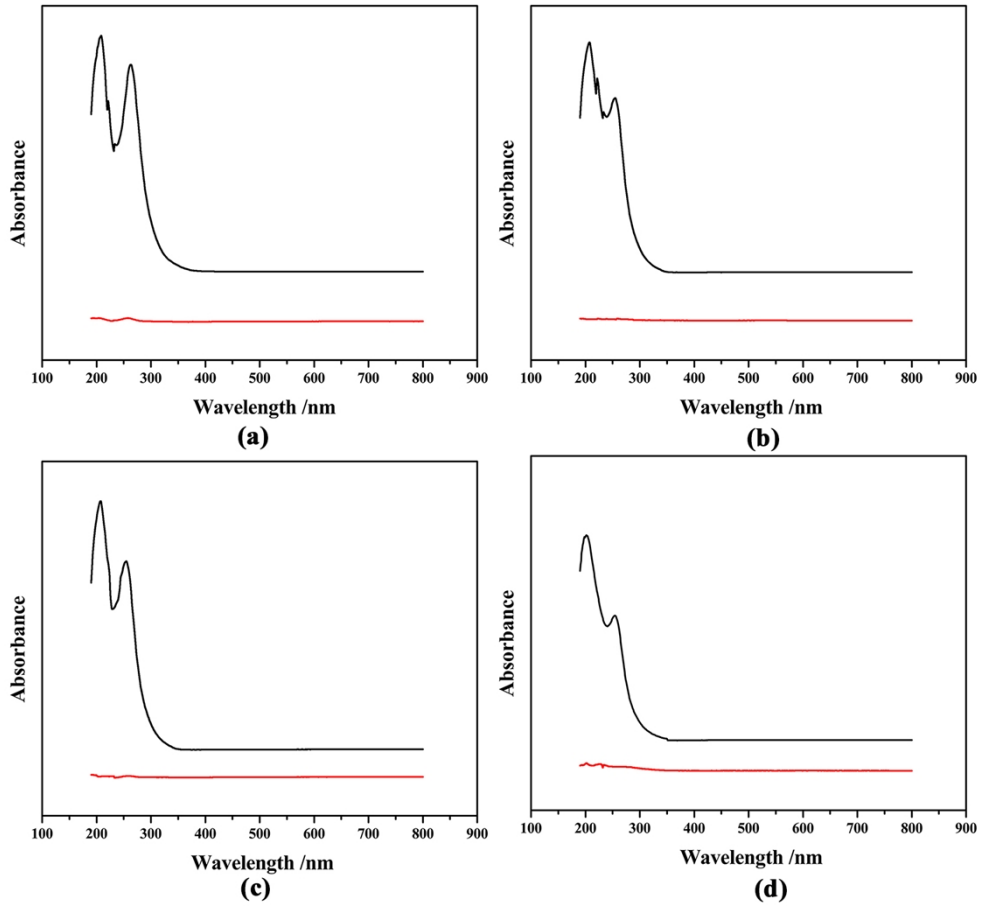

Figure. S21 UV−vis absorption spectra of $K_5[BW_{12}O_{40}]$ (black) and nanocrystal **2** (red) in **(a)** water, **(b)** acetonitrile, **(c)** dichloromethane, **(d)** *n*-octane. These results suggest that $K_5[BW_{12}O_{40}]$ can totally dissolve in H_2O and slightly dissolve in other solvent systems, but all show characteristic peaks in the UV-vis spectra. However, the nanocrystal **2** cannot dissolve in above solvents and no signals can be observed in the UV-vis spectra.

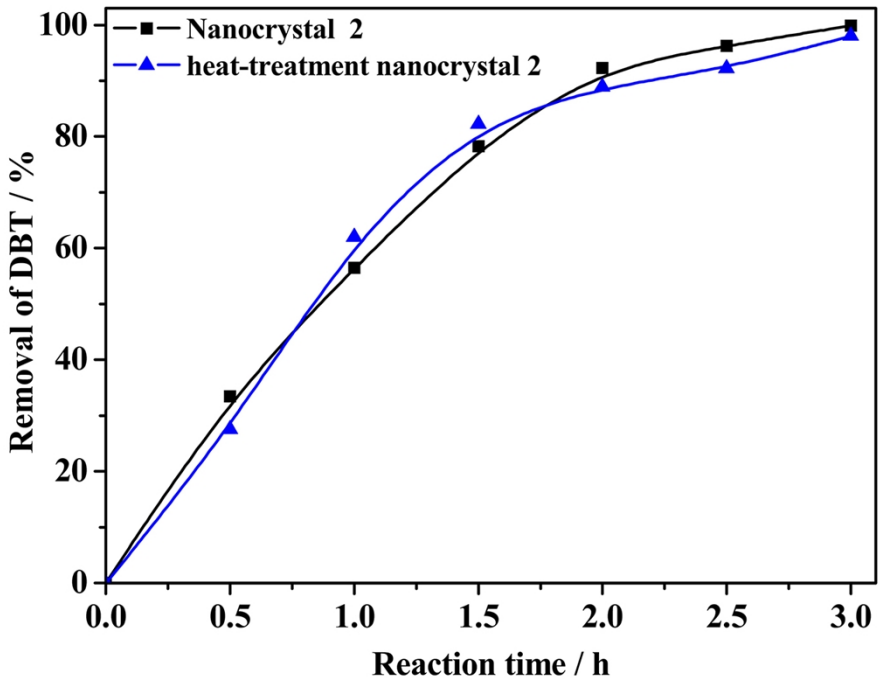

Figure. S22 Removal of DBT versus reaction time by using nano-crystalline **2** and heat-treatment nano-crystalline **2** as catalysts. The nano-crystalline **2** as the representative sample has been heat-treated at 130 °C for 12 h, the heat-treated sample shows the similar catalytic activity to the one of as-prepared nanocrystalline **2**, suggesting that the L-acid center may have no obvious effect on the catalytic activity of the catalyst.

3.3 The preparation of nanocrystal 2.

In a typical process, a mixture of $K_5BW_{12}O_{40}\cdot n\ H_2O$ (0.4 g, 0.13 mmol), $Co(OAc)_2\cdot 4H_2O$ (0.102 g, 0.4 mmol), and BBTZ (0.15 g, 0.625 mmol) was dissolved in 10 mL of distilled water at room temperature and stirred for 0.5 h. The pH of the reaction mixture was adjusted to about 3.0 with 1.0 M HCl. Then, the surfactant hexadecyl trimethyl ammonium bromide (CTAB, 10 mg, 0.027mmol), polyvinyl pyrrolidone (PVP, 10 mg), sodium docecyl sulfate (SDS, 10 mg, 0.035 mmol) was added, respectively. The suspension was sealed in a 23-mL Teflon-lined autoclave and heated at 140 °C for 3 days. After fast cooling to room temperature, the red-brown crystalline solid was filtered, washed with distilled water and ethanol alternately, and dried in an oven at 60 °C for 24 h. The XPRD suggest that powders obtained by using CTAB and PVP were not in agreement with that of the single crystal 2 (Figure S24), while that of SDS are well in agreement with the one of single crystal **2** (Figure S19). It is presumed that the charge and size of the surfactants may affect the final products. Usually, the cationic surfactant for example CTAB has strong electrostatic interaction with the polyoxoanions and wrap the POM untis. The surfactants with large size (for example PVP) may also wrap the ploy oxoanions, which affect the growth of nanocrystals.

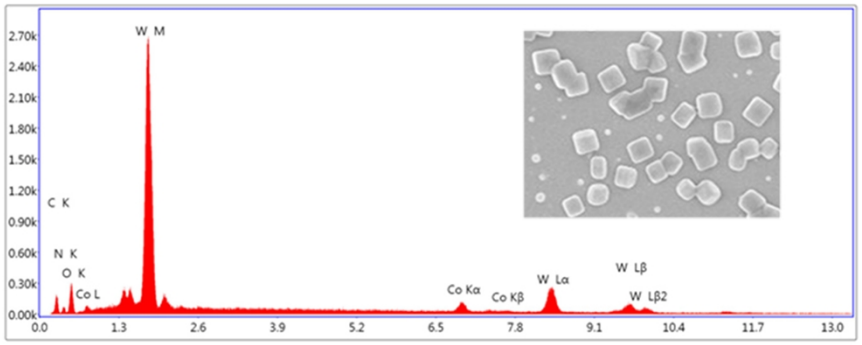

Figure. S23 The EDX spectrums of nanocrystal **2**. The EDX spectra confirmed the main composition of nanocrystal **2** and a Co / W atomic ratio of ~0.2 was suggested by EDX quantitative analysis.

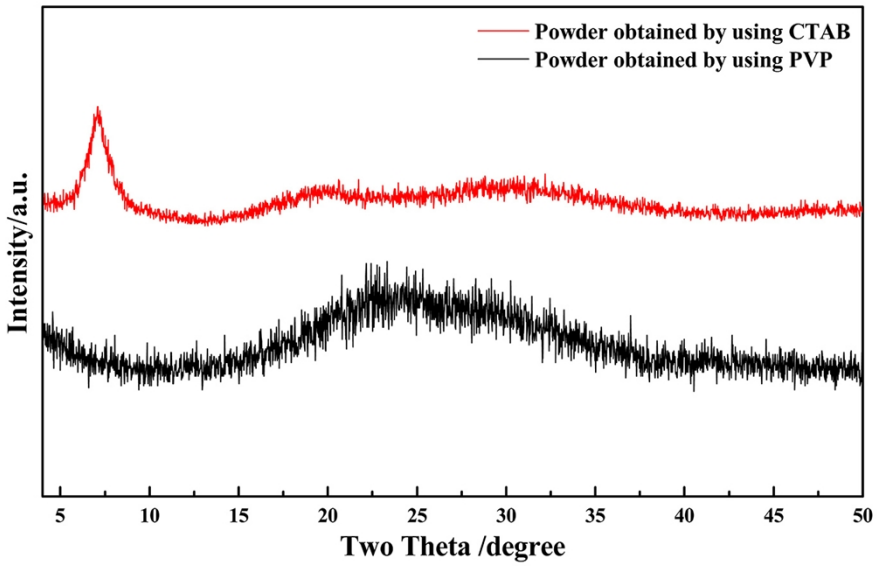

Figure. S24 XPRD patterns of powder obtained by using CTAB(in red) and PVP (in black).

4. Additional physical characterization for compound 1-3

4.1 FT-IR spectra

The IR spectra of **compounds 1-3** are shown in **Figure S25- S27**. In the spectrum of **compound 1**, there are four characteristic peaks of $[PW_{12}O_{40}]^{3-}$ which can be attributed to the vibrations of ν(P-O), ν(W=Od) and ν(W–Ob/c–W) appearing at 1078, 975, 898, 804 cm^{-1}.In the spectrum of **compound 2**, four characteristic peaks of $[BW_{12}O_{40}]^{5-}$ are observed in the range of 1000-700 cm^{-1}. The peaks at 1017 cm^{-1}, 979 cm^{-1}, 924 cm^{-1}, and 799 cm^{-1} are ascribed to the vibrations of ν(B-O), ν(W=Od) and ν(W–Ob/c–W), respectively. In the spectrum of **compound 3**, the characteristic peaks for ν(B-O), ν(W=Od) and ν(W–Ob/c–W) of the polyoxoanion occur at 999 cm^{-1}, 950 cm^{-1}, 902 cm^{-1}, and 821 cm^{-1}. In addition, for this three compounds, the peaks at ca. 3129 cm^{-1} are attributed to to the vibrations of the ν(C-H) in phenyl and triazole rings of BBTZ ligand. Peaks in the regions of 1624-1422 cm-1 may belong to the vibrations of the ν(C=C), ν(C=N) and ν(C=N) in phenyl and triazole rings of BBTZ ligand in **1-3**. The peaks at ca. 3436 cm^{-1} are attributed to the vibrations of $\nu(H_2O)$.

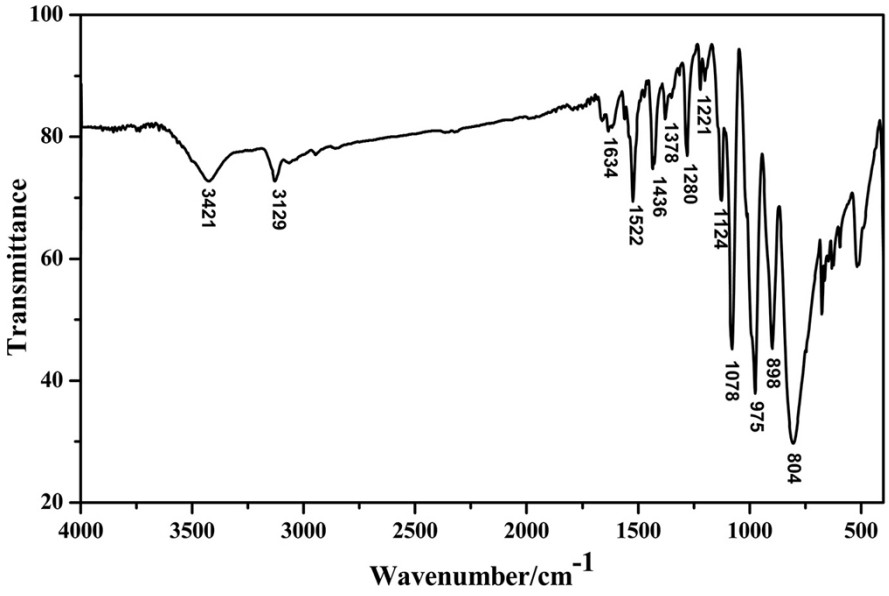

Figure. S25 IR spectrum of **compound 1**.

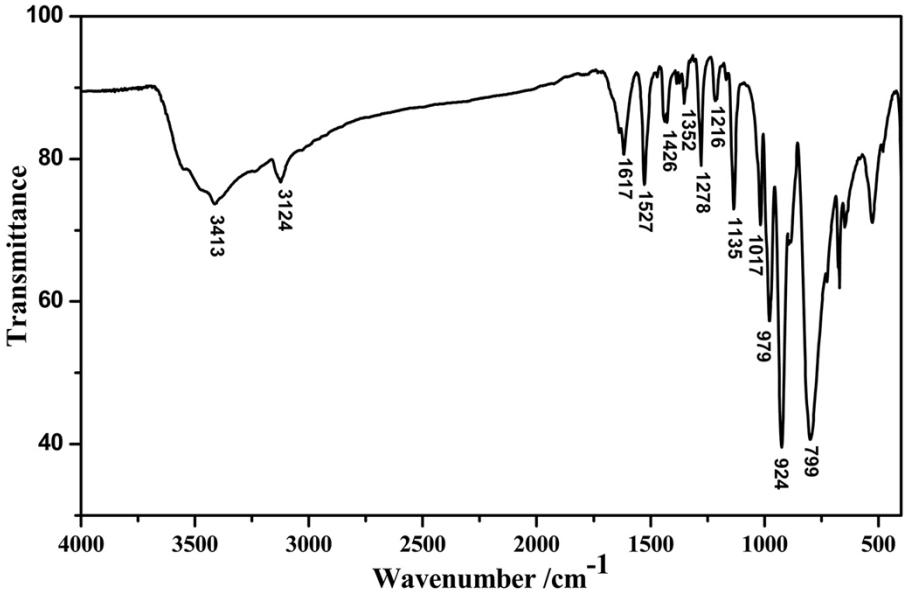

Figure. S26 IR spectrum for **compound 2**.

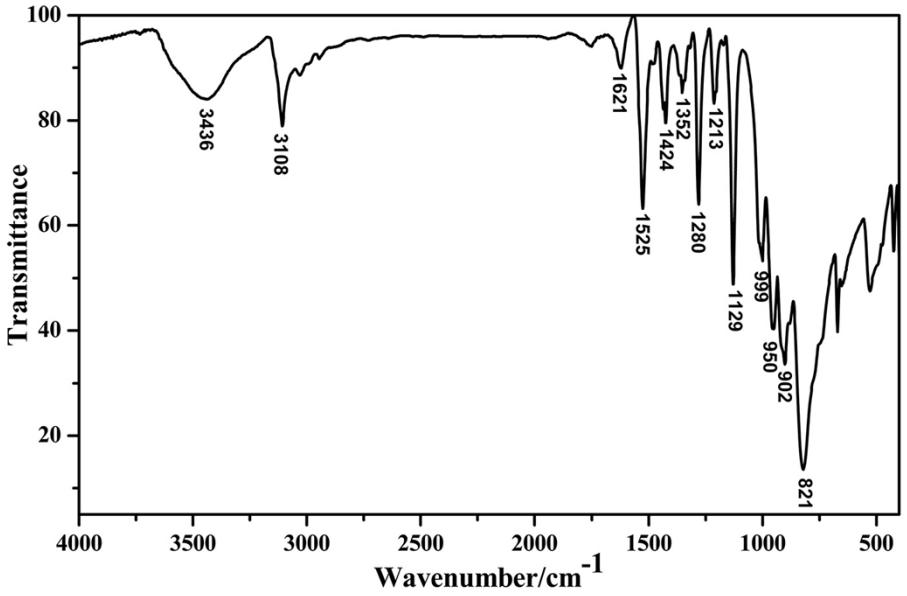

Figure. S27 IR spectrum of **compound 3**.

4.2 Powder X-ray diffractions

In order to check the phase purity of **compounds 1-3**, the PXRD patterns of them were recorded at room temperature. As shown in **Figure. S28-S30**, the peak positions of simulated and experimental patterns of **compounds 1-3** are in agreement with each other, indicating the good phase purity of them. The differences in intensity are due to the preferred orientations of the crystalline powder samples.

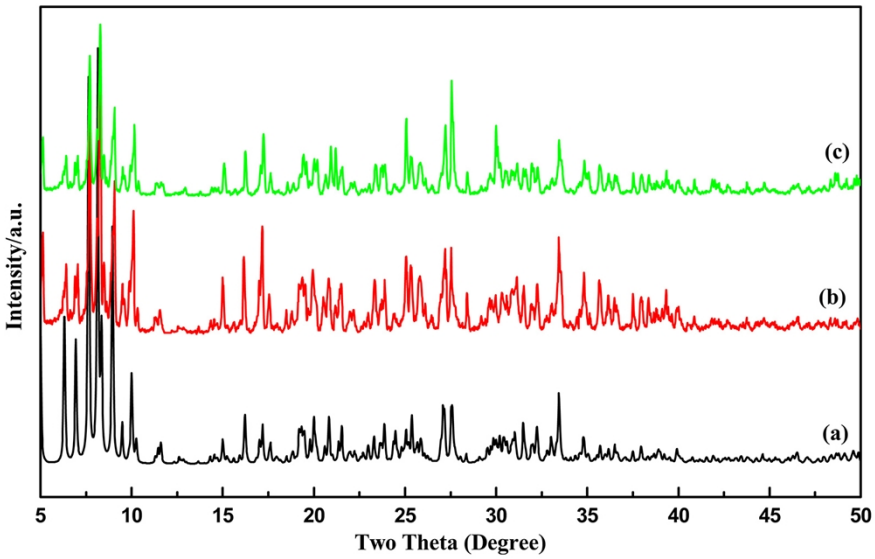

Figure. S28 XPRD patterns of **compound 1**: (a) simulated, (b) as-synthesized, (c) recovered after catalytic reaction of DBT.

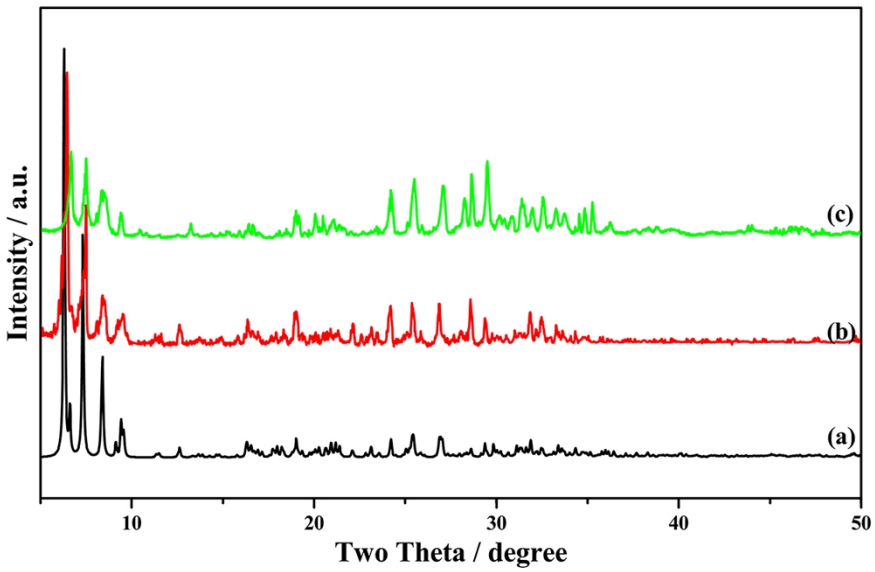

Figure. S29 XPRD patterns of **compound 2**: (a) simulated, (b) as-synthesized, (c) recovered after catalytic reaction of DBT.

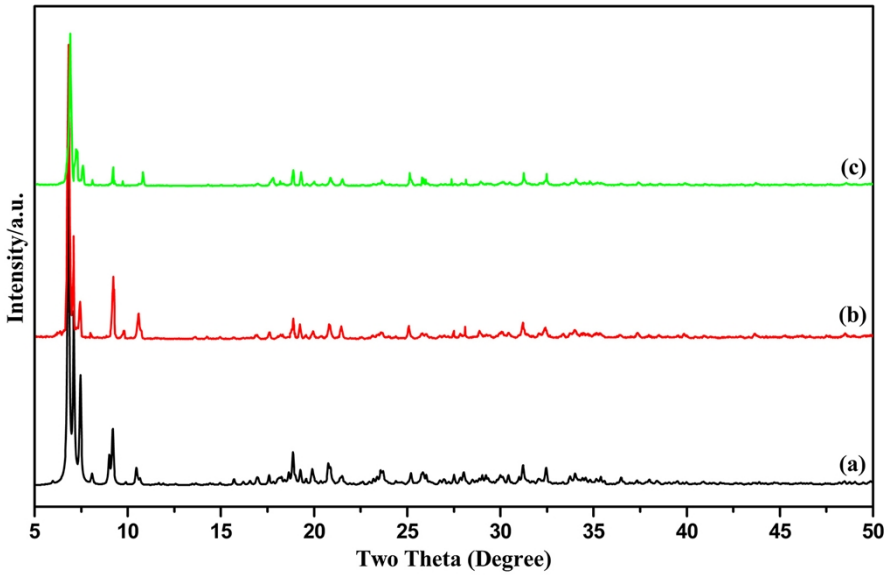

Figure. S30 XPRD patterns of **compound 3**: (a) simulated, (b) as-synthesized, (c) recovered after catalytic reaction of DBT.

4.3 TG Analyses

All TG measurements are performed under the atmosphere of air.

The TG curve of **compound 1** also shows two weight loss stages (**Figure. S31**). The first weight loss of 1.76% in the temperature range of 50 ~ 200℃ corresponds to the loss of one lattice water molecule and two coordinated water molecules (calcd. 1.74%). The second weight loss from 362 ~ 820℃ is ascribed to the loss of C, N atoms and the formation of CoO and WO_3. The whole weight loss of 20.49% is in agreement with the calculated value 20.43%.

The TG curve of **compound 2** shows two weight loss steps (**Figure. S32**). The first weight loss of 2.63% in the temperature range of 50 ~ 210 ℃ corresponds to the loss of four lattice water

molecules and two coordinated water molecules (calculated value 2.65%). The second weight loss of 23.76% from 393 to 791℃ is ascribed to the loss of C, N atoms and the formation of CoO, WO_3 and B_2O_3. The whole weight loss of 26.39% is in agreement with the calculated value 26.21%.
The TG curve of **compound 3** exhibits the first weight loss of 0.84% in the temperature range of 50 ~ 220℃ corresponding to the loss of four lattice water molecules (calcd. 0.85%). The second weight loss in the range of 360 ~780℃ is 29.03% and attributed to the loss of C, N atoms and the formation of CuO, WO_3 and B_2O_3. The whole weight loss of 29.87% is in agreement with the calculated value 29.75% (**Figure S33**).

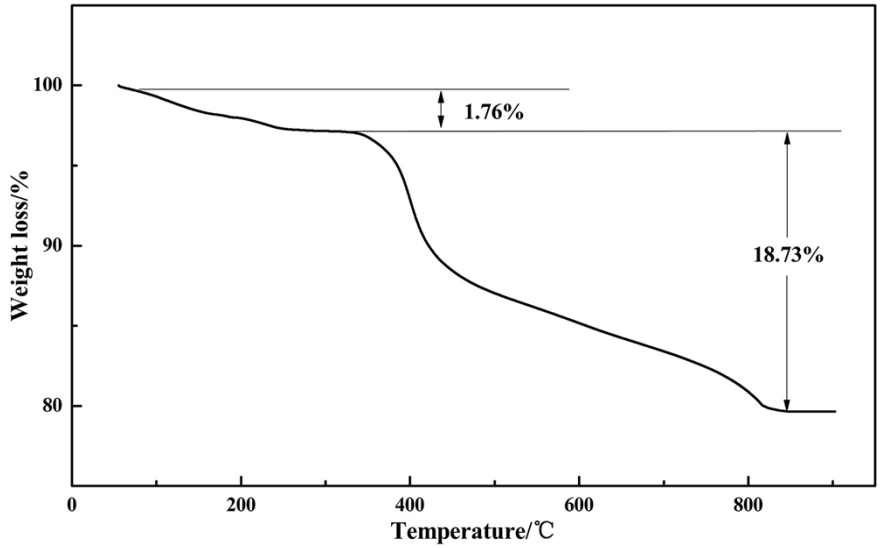

Figure. S31 The TG curve of **compound** 1

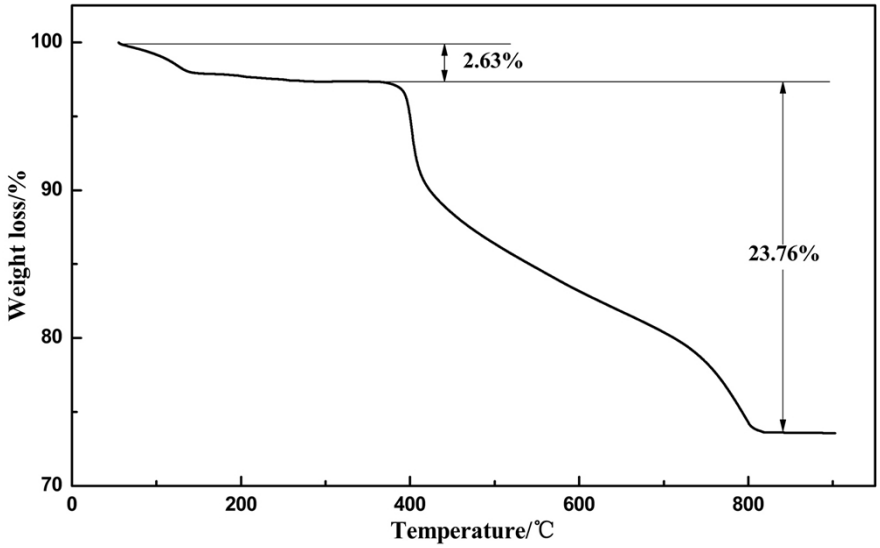

Figure. S32 TG curve of **compound 2**

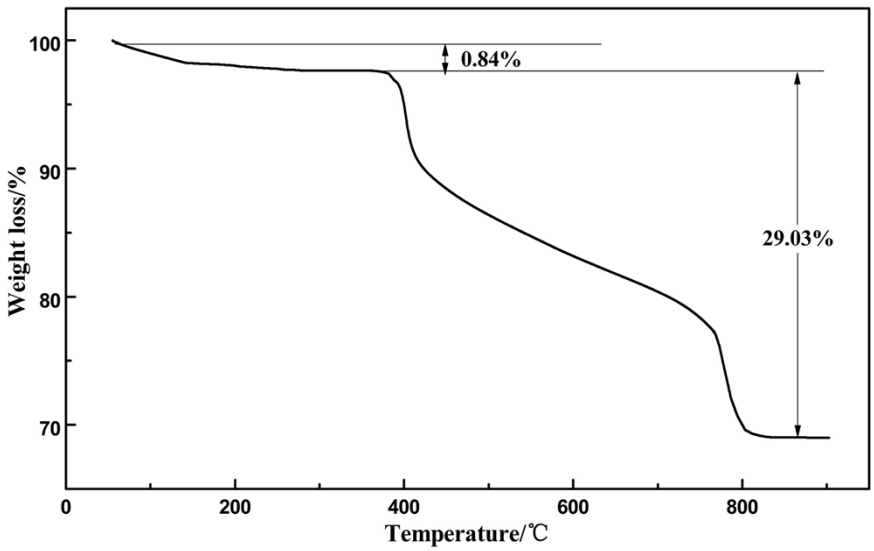

Figure. S33 TG curve of **compound 3**

5. The additional catalytic oxidation experiments of DBT in *n*-octane

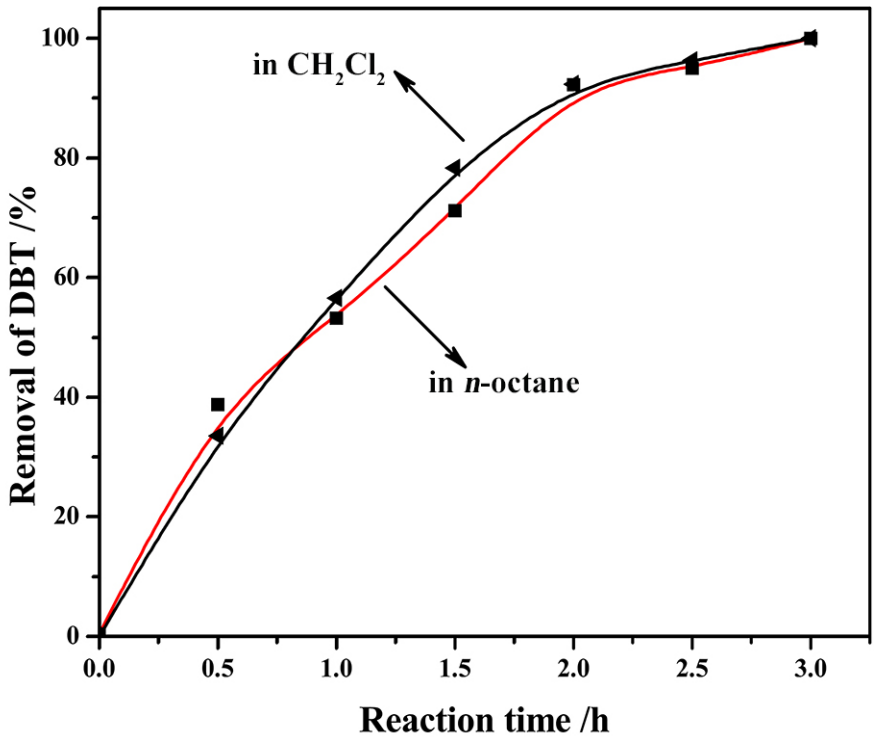

Figure. S34 Removal of DBT versus reaction time by using nano-crystalline **2** as catalyst in *n*-octane and CH_2Cl_2, the results suggest that the nano-crystalline **2** still exhibit good catalytic activity on the oxidation of DBT, which is similar to those in the solvent CH_2Cl_2.

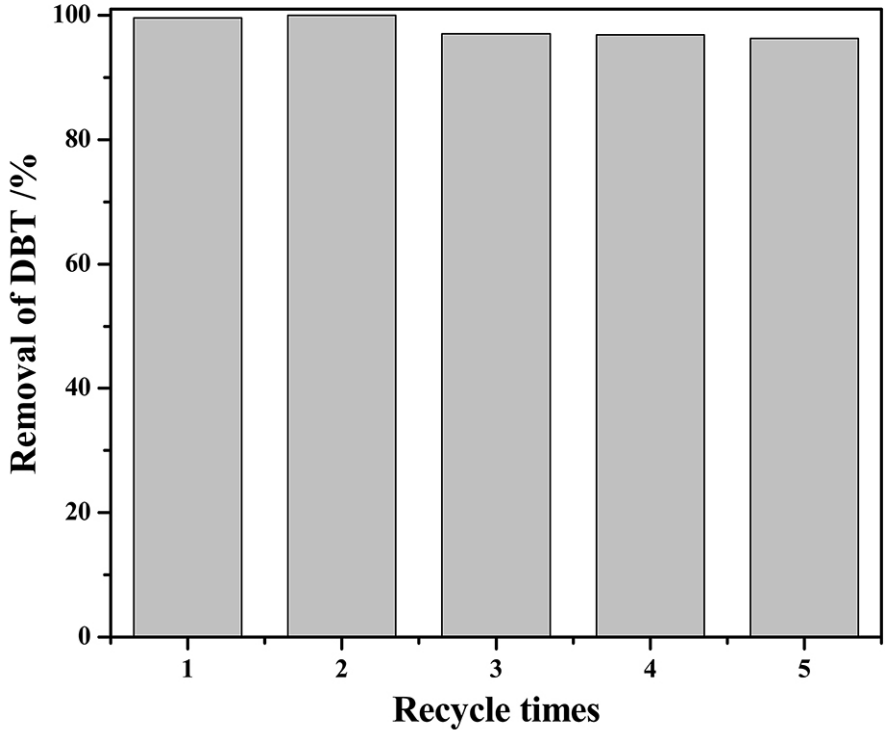

Figure. S35 The recycle experiments with nano-crystalline **2** as catalyst in model oil *n*-octane. The recycling experiments of nano-crystalline **2** in *n*-octane also have been investigated and the conversion of DBT still reached 96.3% after 5-times recycling without a significant decrease The slightly decrease of catalytic activity after reused for five cycles might be related to the slight loss of catalysts in the process of recycle.

Reference

1 X. L. Hao, Y. Y. Ma, H. Y. Zang, Y. H. Wang, Y. G. Li, E. B. Wang, *Chem. Eur. J.,* 2015, **21**, 3778.

2 Y. W. Liu, S. M. Liu, S. X. Liu, D. D. Liang, S. J. Li, Q. Tang, X. Q. Wang, J. Miao, Z. Shi, Z. P. Zheng, *ChemCatChem.,* 2013, **5**, 3086.